NETWORK MODELLING OF INTERNAL AND EXTERNAL GAS DRIVE

Susanne Poulsen(1), Steven R. McDougall(2), Kenneth S. Sorbie(2), and Arne Skauge(3)
(1) Dept of Chemical Engineering, Technical University of Denmark
(2) Heriot-Watt University, Edinburgh, Scotland
(3) Norsk Hydro ASA, Bergen, Norway

ABSTRACT
This paper addresses the issue of analysing relative permeability data specific to the depressurisation process. Relative permeability data from depressurisation experiments are needed for modelling production below bubble point pressure, and for describing near wellbore flow scenarios. Recent experimental studies have proved that gas relative permeability can be several orders of magnitude lower for an internal gas drive process (gas liberation during depressurisation) than for an external gas drive process (gas injection). It has been suggested that phase distribution differences are responsible for this.

The objective of this work was to apply network models for confirming and expanding on the existing experimental observations concerning comparison of internal and external gas drive relative permeability. A systematic series of simulations have been carried out with two different network models. One model simulates an internal gas drive process, and the other simulates an external gas drive process.
Relative permeability curves and critical gas saturations generated by the two network models have been compared. The general trends in the output data were found to compare well with the few existing experimental works that are reported in literature. It was found that gas relative permeability from the external drive process strongly exceeded gas relative permeability from the internal gas drive process. It was found that *pore size distribution*, *coordination number* and *bubble density* are among the factors that control the magnitude of the difference between internal- and external gas drive relative permeability and critical gas saturation. Oil relative permeability was found to be much less affected by the different drive processes, in that oil relative permeability curves from internal and external gas drive simulations practically overlapped. The coordination number seems to be the factor that controls the oil relative permeability in both processes.

INTRODUCTION
The following three existing bodies of work address the issue of comparing relative permeability from internal and external gas drive processes:
  Yortsos and Parlar (1989)[1] performed a theoretical study of the liquid-to-vapour phase change by pressure decline in porous media. The principal issues of super saturation, nucleation and gas-phase growth were examined. It was concluded that for otherwise identical conditions, nucleation events are likely to occur in the larger pore bodies first. The super saturation needed for the appearance of the first bubble was found to be largely independent of features unrelated to the nature of the porous medium, - such as for example the rate of pressure decline. Oil relative permeability resulting from internal and

external gas drive was found to be quite similar. The gas relative permeability on the other hand was lower for internal drive especially at high nucleation densities.

Stewart et al. (1954)[2] compared gas-oil relative permeability ratios resulting from internal and external gas drive experiments. The authors performed experiments on two types of limestone. The authors stated that decreasing the decline rate (thereby decreasing the bubble density) led to a situation where the internal and external gas drive processes show similar behaviour.

Egermann and Vizika (2000)[3] presented oil and gas relative permeability data and critical gas saturation from depressurisation experiments. The flow functions were derived by history matching the experiments with a model that takes the physical phenomena related to gas formation and bubble growth in porous media into account. The internal gas drive relative permeability curves were compared to curves obtained from an external gas injection experiment. The results show that both k_{ro} and k_{rg} depend on the process. k_{ro} values are higher for solution gas drive than for gas injection. This behaviour is attributed to the phase distribution differences between gas injection and solution gas drive. When gas is injected, it invades the largest pores, it is continuous and highly mobile, and, even at low saturations, it inhibits oil flow. In solution gas drive instead, gas bubbles appear next to the pore walls in all pores independently of their size. This gas is initially discontinuous and immobile and gets connected only above a often very high S_{gc}. The trend is reported to be opposite for k_{rg}, in that the curve is several orders of magnitude lower in solution gas drive experiments.

NETWORK MODELLING
The two network models applied in this study are described in the following.
External drive model:
The filling regime that is implemented into the drainage model is an invasion percolation top down algorithm. In this algorithm initially, all bonds are filled with the wetting phase (in this study, oil). In the first percolation step the bonds that have radii equal to or larger than a given value, are temporarily filled with the nonwetting invading phase (in this study, gas). Those temporarily replaced bonds that are connected to the inlet are permanently filled with gas. In the next percolation step bonds with a smaller radius are temporarily gas filled. Those temporarily gas filled bonds that are either directly connected to the inlet, or connected to the inlet by a pathway of other gas filled bonds, will then become permanently gas filled. This procedure continues until the smallest bonds in the network have been considered in the percolation process. Once a gas cluster spans the network, the pressure field is solved and Darcy's law is applied for calculation of relative permeability.

Internal drive model:
The internal drive model simulates the process of depressurising oil, contained in porous media, to pressures below the bubble point pressure. When oil is depressurised below bubble point pressure in a porous medium, bubbles are nucleated in cavities over a range of super saturations. The nucleation model currently implemented in the code is the pre-existing vapour model after Yortsos and Parlar[1]. A fixed number of bubbles are nucleated in the first pressure decline step, and no bubbles nucleate subsequently as pressure

declines. I.e. the model does not incorporate sequential bubble nucleation. The bubbles grow due to expansion and diffusion as pressure declines. Concentration gradients cause gas to diffuse into the nucleation sites. A first-principles multiphase diffusion module is incorporated into the model. For any given pressure step taken in unit time, the new equilibrium gas-oil-ratio (GOR) value is calculated based on inputted curves of pressure versus GOR. By comparing the new GOR value to that of the previous depletion step, the mass of gas that would come out of solution if the system were shut down and allowed to equilibrate is calculated. I.e. the 'available gas mass' is calculated. Diffusion of gas into the bubble-sinks is then calculated over a depletion step and the transferred amount of gas is constantly surveyed. If the amount of transferred gas exceeds the 'available gas mass', then the gas sinks are "plugged" and the system is allowed to equilibrate.

Bubbles grow spherically until constrained by the walls of the bond. The ideal gas law is applied for calculating the bubble radius as a function of temperature, external oil or water pressure and the number of moles of gas present in the bubble. When a bubble outgrows the bond the bubble ceases to grow in a spherical pattern. The bubbles subsequent expansion into the network of surrounding bonds depends upon whether the host-bond is 'constrained' or not. A host bond is constrained if surrounded by neighbouring bonds with smaller radii. When a bubble outgrows a constrained bond, the growth is paused. The bubble volume remains constant while gas diffusion into the bubble causes the bubble pressure to increase. When the bubble pressure exceeds the capillary entry threshold, then growth will resume.

Pressure dependent interfacial tension was applied when describing the bubble growth in the internal model. Oil was allowed to shrink as pressure declined. Temperature was kept constant throughout the simulations.

The growing gas bubbles coalesce into larger clusters, and once buoyancy is big enough, the clusters may start migrating upward in the system. Relative permeability and critical gas saturation (under both spreading and non-spreading conditions) are some of the parameters that are calculated during this type of simulation. More detail on the depressurisation network model is provided by McDougall and Sorbie (1997)[4].

Common features in the two models:
The options for specifying the geometry of the network are more or less the same in both models. All networks applied in this study were three-dimensional cubic networks, in which all bonds were assigned cylindrical geometry. Thus, an exponent of two was applied for scaling the bond volume, and an exponent of four was applied for scaling the hydraulic conductivity. The models apply "throat only" networks, i.e. they are not full bond-site models. The coordination number (average number of open bonds meeting in a junction) specifies the connectivity of the network. The bond size distribution is selected from a list offering ten different probability distribution functions. The radii are distributed in the network by use of a random number generator. Likewise the user-specified coordination number is matched by closing a number of bonds on random locations. Identical networks can be specified in the two network models by feeding the random number generator with the same seed.

Networks with dimension of 15*15*15 bonds (10,350 bonds in total) were applied in all simulations presented in this paper.

Film flow was not included in any of the simulations presented in this paper. In both models, oil becomes trapped if an escape-route of oil filled bonds connecting to the outlet is not available.

SIMULATION SCHEME

The present study focused on comparing relative permeability from internal and external drive simulations in which the *pore size distribution*, the *coordination number* and the *bubble density* was varied. The topology of the network was varied by using four different coordination numbers (Z = 3, 4, 5 and 6). Four different pore size distributions (uniform, log-uniform, truncated normal and cubic) were applied, as shown in Figure 1. As can be seen from Figure 1, the cubic pore size distribution function creates a network with many large bonds and few small bonds. Conversely the log-uniform pore size distribution function creates a network with many small bonds and few large bonds. The truncated normal distribution function creates a pore size distribution resembling that of typical Berea sandstone.

Figure 1 Distribution functions applied for distributing the bond radii in the network
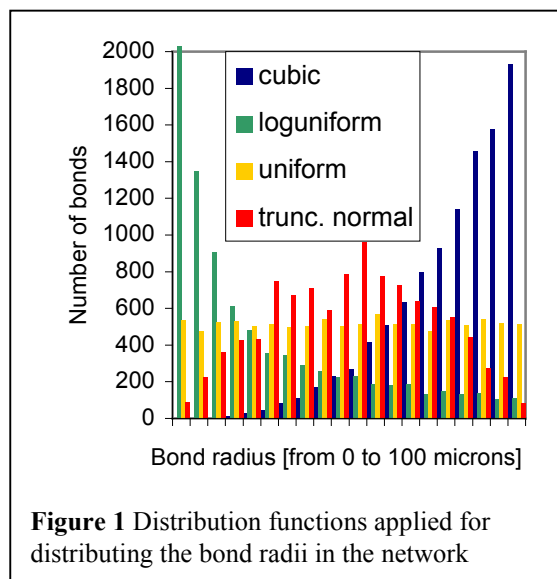
Two different bubble densities (10 and 1000 nucleation sites) were applied. The question of how many bubbles to nucleate at a given pressure decline rate is difficult to answer, because no precise guidelines are found in literature. The following publications present bubble density at various pressure decline rates: Kennedy and Olson (1952)[8], Hunt and Berry (1956)[9], and Firoozabadi and Kashchiev (1993)[10]. No quantitative consensus is reached among these publications, other than the fact that increasing decline rate leads to an increasing number of nucleated bubbles which in turn leads to higher S_{gc} and better oil recovery. Different approaches were taken by the various authors listed above to extend the existing theory on homogeneous bulk nucleation to apply for nucleation in porous media. The reason why no quantitative agreement is formed among these publications is two-fold. First of all, it is difficult to detect and count the actual number of bubbles formed within a 'real' porous medium during a depressurisation experiment. Second of all, different types of porous media were applied in those studies that relied on experimental data, and different so-called shape-factors were applied to account for the topology of the porous medium when modelling the experimental results. The surface structure of the rock, and the amount of impurities in the fluids are among the factors that condition the nucleation density.

By nucleating 10 and 1000 bubbles respectively in the simulations presented in this study, it is possible to compare a situation with high bubble density, to a situation with low bubble density. Both bubble densities are realistic.

SIMULATION RESULTS

Figures 2 and 3 compare oil and gas relative permeability resulting from external and internal drive runs performed with <u>uniform pore size distribution</u>, and with different coordination numbers and different bubble densities. The colour code is chosen such that relative permeability from different simulations performed with the same coordination number has the same colour.

Note that only approximately 600 bubbles were nucleated in the internal drive runs, even though the simulator was preset to nucleate 1000 bubbles. This is due to the fact that not enough bonds in the given networks could satisfy the criteria that two neighbour bonds are not allowed to nucleate, and that bonds on the edge of the network are not allowed to nucleate. The data in Figure 2 show that when a uniform pore size distribution is applied, the coordination number affects oil relative permeability in both the internal and external drive simulations. Furthermore the figure shows that internal and external drive oil relative permeability more or less overlap, independent of whether 10 or >600 bubbles are nucleated.

The gas relative permeability however (Figure 3) is different for external and internal drive when many bubbles are nucleated. Gas relative permeability from internal drive is lower than that for external drive. When only 10 bubbles are nucleated though, the internal and external drive gas relative permeability curves more or less overlap. I.e. k_{rg}(internal 600 bub) < k_{rg}(external) ≈ k_{rg}(internal 10bub). This trend is less pronounced for high coordination numbers.

Figures 4 and 5 compare oil and gas relative permeability resulting from external and internal drive runs performed with <u>truncated normal pore size distribution</u>, and with different coordination numbers and different bubble densities.

The trends exposed in Figure 4 are very similar to the trends exposed for the uniform pore size distribution (Figure 2), namely that internal and external drive oil relative permeability overlap, independently of the bubble density. Figure 5 show that internal and external drive gas relative permeability differs when more than 600 bubbles are nucleated. However the difference between internal and external drive gas relative permeability is not so pronounced in Figure 5 (truncated normal pore size distr.) as it is in Figure 3 (uniform pore size distr.).

Figures 6 and 7 compare oil and gas relative permeability resulting from external and internal drive runs performed with <u>log-uniform pore size distribution</u>, and with different coordination numbers and different bubble densities.

The oil relative permeability curves resulting from runs with log-uniform pore size distribution (Figure 6) follow the same trends that are seen in Figure 2 (uniform pore size distr.) and Figure 4 (truncated normal pore size distr.). I.e. oil relative permeability from

internal and external drive runs practically overlap when the log-uniform pore size distribution is applied.

The gas relative permeability resulting from runs with log-uniform pore size distribution (Figure 7) also exhibits the same trends as those revealed for the uniform (Figure 3) and truncated normal (Figure 5) pore size distribution. However the trends are more pronounced for the log-uniform pore size distribution than for the two former pore size distributions. Gas relative permeability from internal drive with >600 bubbles nucleated is much lower than it is in the internal drive run with 10 bubbles nucleated and in the external drive run. This is true for all coordination numbers, meaning that internal drive gas relative permeability seems to be independent of coordination number when many bubbles are nucleated in a network with log-uniform pore size distribution.

Finally, Figures 8 and 9 compare oil and gas relative permeability resulting from external and internal drive runs performed with <u>cubic pore size distribution</u>, and with different coordination numbers and different bubble densities.

As shown in Figure 8, again the oil relative permeability is identical for external and internal drive runs, independently of the number of bubbles nucleated.
The same is true for the gas relative permeability (Figure 9), except for the runs that applied a coordination number of three. I.e. unlike the uniform-, truncated normal- and log-uniform distributed networks; internal and external drive gas relative permeability almost overlaps when a cubic pore size distribution is applied – also for the high bubble density.
Another factor that separates Figure 9 from the three previous gas relative permeability figures is that the relative permeability curves are ranked according to the coordination number. At low oil saturations the gas relative permeability resulting from runs with coordination number of six are higher than those resulting from runs with coordination number of five, which again are higher than those resulting from runs with coordination numbers of four and three. In other words, the gas relative permeability originating from runs with a cubic pore size distribution are not ranked such that internal drive gas relative permeability is higher than external drive gas relative permeability, but instead ranked according to coordination number.

SUMMARY OF OBSERVATIONS BASED ON FIGURES 2 – 9:
Common for the eight figures that have been discussed above is that the relative permeability data corresponding to a coordination number of three look somewhat distorted. The most likely explanation for this is that these simulations are performed on networks that are too small. When specifying a coordination number of three, half of the bonds in the network become closed.
The following preliminary observations have been extracted based on the results shown through Figures 2 to 9 (curves resulting from simulations that applied a coordination number of three are disregarded):

Concerning oil relative permeability:
- For similar networks, k_{ro} seems to be more or less identical for internal and external drive simulations.

Concerning gas relative permeability:
- k_{rg} resulting from external drive simulations is higher than or equal to k_{rg} resulting from internal drive simulations.
- **Pore size distribution:** The network modelling results show that the largest difference between external and internal drive k_{rg} seems to be obtained when the pore size distribution is log-uniform, i.e. most small bonds. The smallest difference between external and internal drive k_{rg} seems to be obtained when the pore size distribution is cubic, i.e. most large bonds. When applying the uniform and the truncated normal pore size distribution, the difference between internal and external drive k_{rg} is 'intermediate', - i.e. more pronounced than when applying the cubic pore size distribution, and less pronounced than when applying the log-uniform pore size distribution.
- **Bubble density:** The results also show that the deviation between internal and external drive k_{rg} is dependent on bubble density. The higher the bubble density, the larger the deviations between internal and external drive k_{rg}. When only 10 bubbles are nucleated, the internal and external drive gas relative permeabilities practically overlap.
- **Coordination number:** Finally the results show that the deviation between internal and external drive k_{rg} is dependent on the connectivity of the network (coordination number). The higher the coordination number, the smaller the deviation between internal and external drive k_{rg}. The lower the coordination number, the larger the gap between internal and external drive k_{rg}.

In order to enhance the visualization of the trends just reported, and to extract additional information from the simulations, some of the simulation data are now shown in plots where relative permeability from simulations performed with the same coordination number are compared. I.e. relative permeability curves resulting from simulations with different pore size distributions are plotted in the same figure. By doing so, the effect of pore size distribution on relative permeability is easier to see.

Figures 10 and 11 compare oil and gas relative permeability resulting from external and internal drive runs performed with a coordination number of six and with different pore size distributions and different bubble densities. The data in Figure 10 confirm that oil relative permeability from internal drive runs and external drive runs overlap when Z=6. The data also show that oil relative permeability is not completely unaffected by the pore size distribution applied in the network. At high oil saturations the oil relative permeability resulting from the log-uniform runs is lower than when applying uniform-, cubic or truncated normal pore size distribution. In other words, at high oil saturations the oil relative permeability is lowest for the network that contains most *small* bonds. At low oil saturations however, the picture is reversed. I.e. at low oil saturations the oil relative permeability is lowest for the network that contains most *large* bonds.
The gas relative permeability data in Figure 11 confirm the observations already reported, namely that gas relative permeability resulting from internal and external drive runs almost overlap at low bubble density (10 bubbles), but differ strongly at high bubble density

(>600 bubbles). The data in Figure 11 also serves to validate the observation that internal drive gas relative permeability deviates more from external drive gas relative permeability when the network contain most small bonds (log-uniform pore size distr.) than when the network contain most large bonds (cubic pore size distr.).

Figures 12 and 13 compare oil and gas relative permeability resulting from external and internal drive runs performed with <u>a coordination number of five</u> and with different pore size distributions and different bubble densities. The oil relative permeability data in Figure 12 (coordination number of five) exhibit the same trends as those in Figure 10 (coordination number of six). The gas relative permeability data in Figure 13 (coordination number of five) however differ from the gas relative permeability curves shown in Figure 11, in that the pore size distribution has a more pronounced effect on the deviation between external and internal drive curves. I.e. it is validated that when lowering the coordination number, the gas relative permeability curves resulting from internal drive become more sensitive to the pore size distribution applied. This trend is confirmed by the data shown in Figure 14. Figure 14 compares gas relative permeability resulting from external and internal drive runs performed with <u>a coordination number of four</u> and with different pore size distributions and different bubble densities.

Oil relative permeability curves resulting from runs with coordination number of four are not shown here, as this plot contains no new information. It merely repeats the trends that are shown in Figure 10 (coordination number of six) and in Figure 12 (coordination number of five).

SUMMARY OF OBSERVATIONS BASED ON FIGURES 10 – 14:
The following observations have been extracted based on the results shown in Figures 10 to 14:

Concerning oil relative permeability:
- **Pore size distribution**: Both internal and external drive k_{ro} is affected by pore size distribution. But not to the same extent as the gas relative permeability. For coordination numbers above three, different patterns can be observed at high oil saturation, than at low oil saturation. *At high oil saturation* the same trend is exhibited as in gas relative permeability, i.e. the highest internal drive k_{ro} originates from the network that contains most large bonds (cubic pore size distribution). Inversely, the lowest internal drive k_{ro} originates from the network that contains most small bonds (log-uniform pore size distribution). *At low oil saturation* the opposite trend is observed. I.e. the highest k_{ro} is produced with the network that contains most small bonds, and the lowest k_{ro} is produced with the network that contains most large bonds.

Concerning gas relative permeability:
- **Pore size distribution**: The plots in Figure 11, 13 and 14 confirmed that internal drive k_{rg} is affected by pore size distribution while external drive k_{rg} seems to be more or less independent of pore size distribution. The general trend, for coordination numbers above three, is that the network that contains most large bonds (cubic pore size distribution) produces the highest internal drive k_{rg} curves. Inversely, the network that contains most small bonds (log-uniform pore size distribution) produces the lowest internal drive k_{rg} curves.

- **Bubble density**: The plots in Figure 11, 13 and 14 confirmed that internal drive k_{rg} from runs made with high bubble density are more affected by pore size distribution than internal drive k_{rg} from runs with low bubble density.

DISCUSSION

Having now presented the simulation results, and reported the trends that can be observed, the question that remains to be answered is whether these results are merely appropriate for comparing two theoretical models, or whether the data are actually representative for comparing two 'real life' physical processes? Part of the answer to this question is that the results reported in this paper only provide qualitative information on the issue of comparing external and internal drive processes. As no anchoring to experimental data has been performed, no quantitative information may be deduced; - the study was aimed at investigating overall trends. The following overall trends, reported from already existing experimental studies, have been reproduced:

'*Pore topology and bubble density conditions whether internal and external drive processes yield the same recovery behaviour*', (Stewart et al., 1954)[2]. This observation has been reproduced and extended in this simulation study.

'*External drive gas relative permeability exceeds internal drive gas relative permeability by several orders of magnitude. It is suggested that phase distribution differences are responsible for this*', (Egermann and Vizika, 2000)[3]. This observation has been reproduced in this simulation study. See Figures 3, 5, 7 and 9.

'*Internal drive oil relative permeability exceeds external drive oil relative permeability, however the difference is not nearly as pronounced as it is in the gas relative permeability*'. (Egermann and Vizika, 2000)[3]. This observation has not been reproduced in this study; in that oil relative permeability resulting from internal and external drives practically overlap. See Figures 2, 4, 6 & 8.

'*Critical gas saturation resulting from internal drive exceeds critical gas saturation resulting from external drive*'. (Kamath and Boyer, 1993)[5]. This observation has been reproduced in this study; in that internal drive S_{gc} exceeds external drive S_{gc} if the bubble density is high in the internal drive simulation. For low bubble density the opposite is true.

'*The higher the pressure decline rate (i.e. the more bubbles nucleated), the higher the critical gas saturation*'. (Moulu, 1988)[6]. This observation has been reproduced in this study.

It is suggested that the gas phase is distributed differently in the cubic and the log-uniform networks. In the cubic network most of the gas is present within the spanning gas cluster. I.e. the gas phase is well connected due to the fact that the bubbles can expand through large bonds where capillary pressure is low. In the log-uniform network, it is suggested that a number of isolated gas islands surround the spanning gas cluster, due to the fact that some bubbles are constrained from expanding through small bonds where capillary pressure is high. The more bubbles nucleated, the more isolated gas islands. The lower the coordination number, - the longer the diffusion pathways, - the more the isolated gas islands.

CONCLUSIONS

A comparison of the external gas drive process (steady state gas injection) and the internal gas drive process (gas liberation during depressurisation) has been performed. The comparative study was based on network modelling. The network simulations have been found to reproduce a majority of the overall trends reported in literature. The existing knowledge on which factors control the degree of difference between relative permeability curves resulting from internal and external gas drive has been confirmed and extended with the following observations:

1. Pore size distribution is one on the factors that conditions how large the difference between internal and external drive gas relative permeability is. The best match between internal and external drive k_{rg} is obtained when the network contains many large bonds and few small bonds (cubic psd). The worst match between internal and external drive k_{rg} is obtained when the network contains many small bonds and few large bonds (log-uniform psd).
2. Coordination number is also one of the factors that conditions how large the difference between internal and external drive gas relative permeability is. The higher the coordination number, the less the difference between internal and external drive gas relative permeability.
3. Finally bubble density is among the factors that conditions how large the difference between internal and external drive gas relative permeability is. The more bubbles are nucleated, the larger the difference between the internal and the external drive gas relative permeability.
4. Based on these observations it is recommended that internal drive gas relative permeability data should not be generated by extending an external drive relative permeability curve to a critical gas saturation measured in a depressurisation experiment. Internal drive gas relative permeability should be measured in an experiment of its own. Information on relative permeability determination during depressurisation experiments is given by Egermann and Vizika[3] and Naylor et al.[7]. However, if forced to apply external gas drive data for creating an internal gas drive relative permeability curve, the best results will be generated for rock types that have high coordination numbers and a pore size distribution with many large pores and few small pores (cubic type). Dullien[11] discusses how to determine pore size distribution and coordination number.

REFERENCES

1. Yortsos, Y. C., and Parlar, M. (1989). *Phase Change in Binary Systems in Porous Media: Application to Solution-Gas Drive*. Prepared for presentation at the 64th annual Technical Conference and Exhibition of the Society of Petroleum Engineers, San Antonio, TX, Oct. 8-11. SPE19697.
2. Stewart, C. R., Hunt, Jr., E. B., Schneider, F. N., Geffen, T. M., and Berry, Jr. V. J. (1954). *The Role of Bubble Formation in Oil Recovery by Solution Gas Drives in Limestones*. Trans. AIME 201: 560-567. SPE410-G.
3. Egermann, P., Vizika, O. (2000). *A new Method to Determine Critical Gas saturation and Relative Permeability During Depressurisation in the Near-Wellbore Region*. Soc. Core Analyst. Proceedings, Oct. 18-22, 2000. SCA 36-(1).
4. McDougall, S. R, and Sorbie, K. S. (1997). *Estimation of Critical gas Saturation During Pressure Depletion in Virgin and Waterflooded Reservoirs*. Presented at the 9th European Symposium on Improved Oil Recovery, The Hague, The Netherlands, 20-22 Oct. 1997.
5. Kamath, J, and Boyer, R. E. (1993). *Critical Gas Saturation and Supersaturation in Low Permeability Rocks*. Presented at the 68th Annual Technical Conference and Exhibition of the Society of Petroleum Engineers, Houston, Texas, 3-6 October 1993. SPE26663.

6. Moulu, J. C. (1988). Solution Gas Drive: Experiments and Simulation. J. Petr. Sci. Eng., 2: 379-386.
7. Naylor, P., Mogford, D., and Smith, R. (2000). Development of In-situ Measurements to Determine Reservoir Condition Critical Gas Saturations During Depressurisation. Soc. Core Analysts, SCA 2000-37-(1).
8. Kennedy, H. T., and Olson, C. R. (1952). *Bubble Formation in Supersaturated Hydrocarbon Mixtures*. Petr. Trans. AIME, 195: 271-278. SPE 232-G.
9. Hunt, Jr., E. B., and Berry, Jr., V. J. (1956). *Evolution of Gas from Liquids Flowing Through Porous Media*. AIChE J 2: 560-567.
10. Firoozabadi, A., and Kashchiev, D. (1993). Pressure and Volume Evolution During Gas Phase Formation in Solution Gas Drive Processes. Soc. Petr. Eng. SPE26286.
11. Dullien, F. A. L. (1992). *Porous Media: fluid transport and pore structure*. Second edition. ISBN 0-12-223651-3. Academic Press, INC. Pore size distr: p 33. Coordination no.: p. 22.

ACKNOWLEDGMENTS
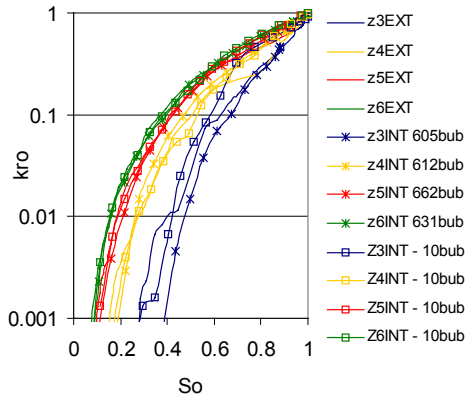
Figure 2 Oil relative permeability from internal and external simulations with <u>uniform</u> pore size distribution. Coordination numbers of Z = 3, 4, 5 and 6 were applied. Bubble densities of 10 and 1000 were applied.
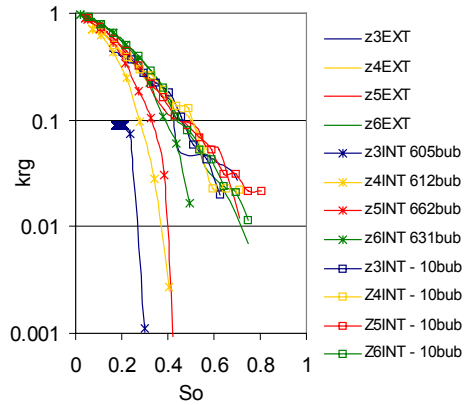
Figure 3 Gas relative permeability from internal and external simulations with <u>uniform</u> pore size distribution. Coordination numbers of Z = 3, 4, 5 and 6 were applied. Bubble densities of 10 and 1000 were applied.
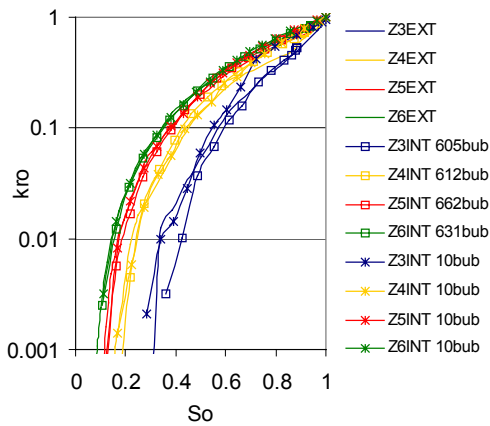
Figure 4 Oil relative permeability from internal and external simulations with <u>truncated normal</u> pore size distribution. Coordination numbers of Z = 3, 4, 5 and 6 were used. Bubble densities of 10 and 1000 were used.
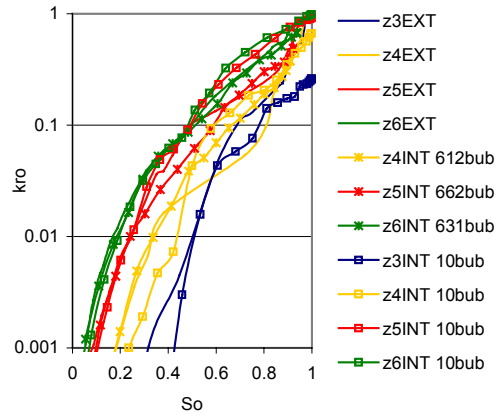
Figure 6 Oil relative permeability from internal and external simulations with <u>log-uniform</u> pore size distribution. Coordination numbers of Z = 3, 4, 5 and 6 were used. Bubble densities of 10 and 1000 were used.
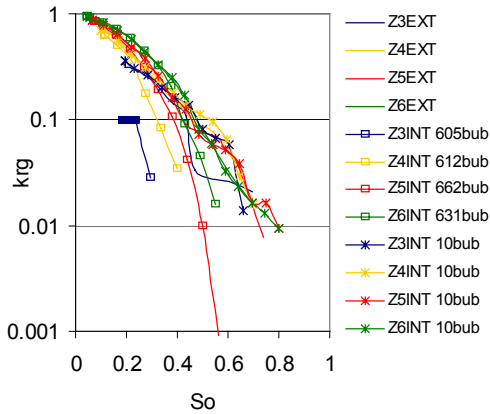
Figure 5 Gas relative permeability from internal and external simulations with <u>truncated normal</u> pore size distribution. Coordination numbers of Z = 3, 4, 5 and 6 were used. Bubble densities of 10 and 1000 were used.
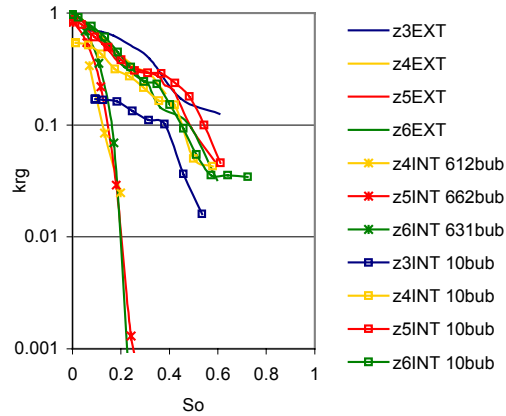
Figure 7 Gas relative permeability from internal and external simulations with <u>log-uniform</u> pore size distribution. Coordination numbers of Z = 3, 4, 5 and 6 were used. Bubble densities of 10 and 1000 were used.
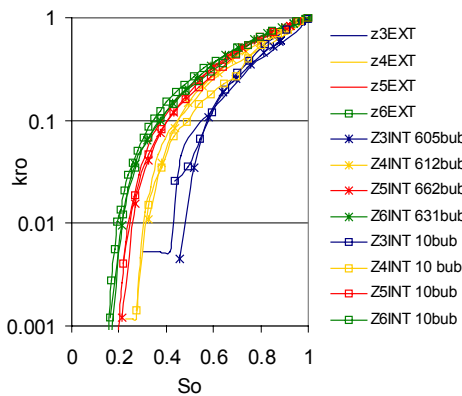
Figure 8 Oil relative permeability from internal and external simulations with <u>cubic</u> pore size distribution. Coordination numbers of Z = 3, 4, 5 and 6 were used. Bubble densities of 10 and 1000 were used.
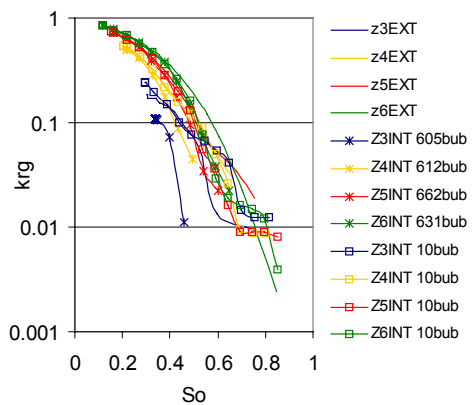
Figure 9 Gas relative permeability from internal and external simulations with <u>cubic</u> pore size distribution. Coordination numbers of Z = 3, 4, 5 and 6 were used. Bubble densities of 10 and 1000 were used.
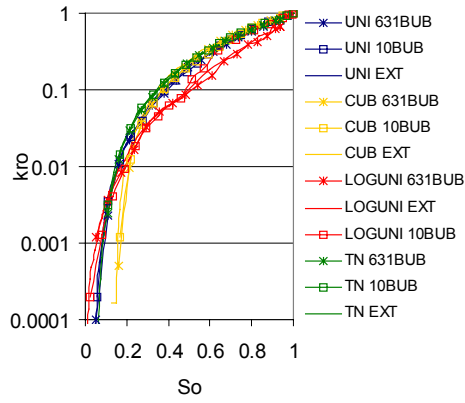
Figure 10 Oil relative permeability from internal and external simulations with <u>coordination number of six</u>. Four different pore size distributions were used. Bubble densities of 10 and 1000 were used.
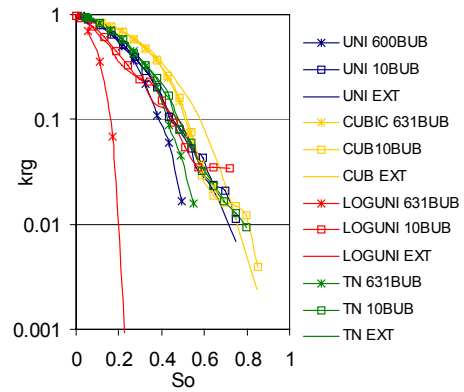
Figure 11 Gas relative permeability from internal and external simulations with <u>coordination number of six</u>. Four different pore size distributions were used. Bubble densities of 10 and 1000 were used.
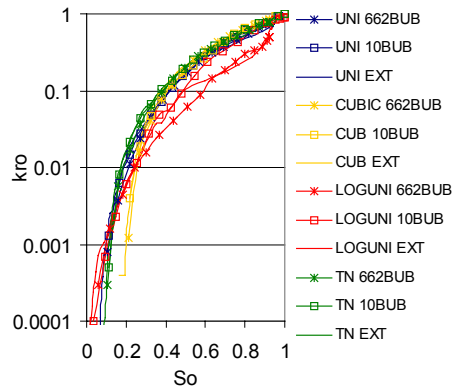
Figure 12 Oil relative permeability from internal and external simulations with <u>coordination number of five</u>. Four different pore size distributions were used. Bubble densities of 10 and 1000 were used.
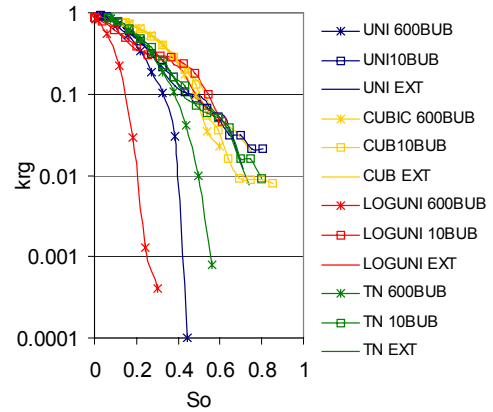
Figure 13 Gas relative permeability from internal and external simulations with <u>coordination number of five</u>. Four different pore size distributions were used. Bubble densities of 10 and 1000 were used.
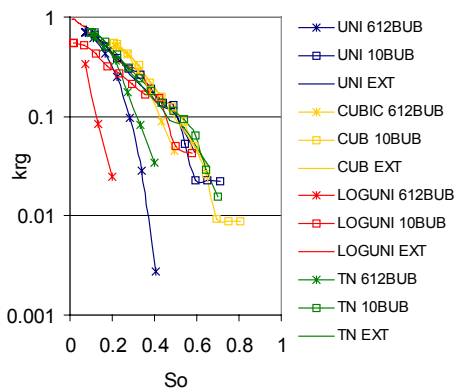
Figure 14 Gas relative permeability from internal and external simulations with <u>coordination number of four</u>. Four different pore size distributions were used. Bubble densities of 10 and 1000 were used.